

MIT Open Access Articles

Optogenetic skeletal muscle-powered adaptive biological machines

The MIT Faculty has made this article openly available. **Please share** how this access benefits you. Your story matters.

Citation: Raman, Ritu, Caroline Cvetkovic, Sebastien G. M. Uzel, Randall J. Platt, Parijat Sengupta, Roger D. Kamm, and Rashid Bashir. "Optogenetic Skeletal Muscle-Powered Adaptive Biological Machines." *Proc Natl Acad Sci USA* 113, no. 13 (March 14, 2016): pp. 3497-3502. © 2016 National Academy of Sciences.

As Published: <http://dx.doi.org/10.1073/pnas.1516139113>

Publisher: National Academy of Sciences (U.S.)

Persistent URL: <http://hdl.handle.net/1721.1/105099>

Version: Final published version: final published article, as it appeared in a journal, conference proceedings, or other formally published context

Terms of Use: Article is made available in accordance with the publisher's policy and may be subject to US copyright law. Please refer to the publisher's site for terms of use.



Optogenetic skeletal muscle-powered adaptive biological machines

Ritu Raman^{a,b}, Caroline Cvetkovic^{b,c}, Sebastien G. M. Uzel^d, Randall J. Platt^e, Parijat Sengupta^{c,f}, Roger D. Kamm^{d,e}, and Rashid Bashir^{b,c,1}

^aDepartment of Mechanical Science and Engineering, University of Illinois at Urbana–Champaign, Urbana, IL 61801; ^bMicro and Nanotechnology Laboratory, University of Illinois at Urbana–Champaign, Urbana, IL 61801; ^cDepartment of Bioengineering, University of Illinois at Urbana–Champaign, Urbana, IL 61801; ^dDepartment of Mechanical Engineering, Massachusetts Institute of Technology, Cambridge, MA 02139; ^eDepartment of Biological Engineering, Massachusetts Institute of Technology, Cambridge, MA 02139; and ^fBeckman Institute for Advanced Science and Technology, University of Illinois at Urbana–Champaign, Urbana, IL 61801

Edited by Stephen R. Quake, Stanford University, Stanford, CA, and approved February 11, 2016 (received for review August 13, 2015)

Complex biological systems sense, process, and respond to their surroundings in real time. The ability of such systems to adapt their behavioral response to suit a range of dynamic environmental signals motivates the use of biological materials for other engineering applications. As a step toward forward engineering biological machines (bio-bots) capable of nonnatural functional behaviors, we created a modular light-controlled skeletal muscle-powered bioactuator that can generate up to 300 μN (0.56 kPa) of active tension force in response to a noninvasive optical stimulus. When coupled to a 3D printed flexible bio-bot skeleton, these actuators drive directional locomotion (310 $\mu\text{m/s}$ or 1.3 body lengths/min) and 2D rotational steering ($2^\circ/\text{s}$) in a precisely targeted and controllable manner. The muscle actuators dynamically adapt to their surroundings by adjusting performance in response to “exercise” training stimuli. This demonstration sets the stage for developing multicellular bio-integrated machines and systems for a range of applications.

bioactuator | stereolithography | tissue engineering | soft robotics

Understanding complex biological systems requires uncovering the mechanisms through which integrated multicellular networks accomplish sensing, internal processing, and coordinated action in response to dynamic environmental signals. Attempting to reverse engineer these mechanisms for applications in regenerative medicine has been the focus of the burgeoning field of tissue engineering (1), and seminal advances in this field have targeted nearly every organ system in the body (2). These developments, in addition to improving the state of the art in therapeutics, have furthered our understanding of the design principles governing the organizational structure and function of natural biological systems. With this as a guide, we are ideally poised to start forward engineering biological machines, or bio-bots, capable of complex controllable nonnatural functional behaviors, thereby broadening the potential applications for building with biological materials.

Before we can design bio-integrated machines for a range of applications, we must first engineer modular tissue building blocks that respond to external signals with complex functional behaviors. Observing and controlling the coordinated action of such building blocks in series and parallel will help us understand the emergent behavior of natural biological systems (3, 4). Nearly all machines require actuators, modules that convert energy into motion, to produce a measurable output in response to input stimuli. Efforts to manufacture bio-integrated actuators have targeted a range of cell types (5), including flagellated bacteria (6), cardiac muscle (7–9), and skeletal muscle (10–12). We previously demonstrated a millimeter-scale soft robotic device, or bio-bot, that uses the contractile force produced by electrically paced skeletal muscle to drive locomotion across a substrate (10). This bio-bot was the first demonstration of an untethered locomotive skeletal muscle powered biological machine and set the stage for building hierarchical actuators inspired by natural systems. However, like other previous demonstrations of bio-integrated machines,

the actuator was coupled to the surrounding device and did not allow for unrestricted use in a variety of design applications. A significant step forward in this field thus requires a modular bioactuator that demonstrates a variety of controllable and tunable functional behaviors in response to a noninvasive external signal.

Here, we present a bioactuator that can be coupled to many different mechanical bio-bot skeletons to provide a desired contractile force output. Two major design advances enable forward engineering bio-bots capable of more complex behaviors: (i) skeletal muscle cells are transduced to express a light sensitive cation channel, using an existing protocol (these optogenetic cells demonstrated controlled contractility in response to noninvasive and spatiotemporally precise optical stimuli); and (ii) muscle actuators are redesigned as “rings” that can be readily coupled to a variety of bio-bot skeleton designs. The resulting bioactuators produced paced active tension forces approaching 300 μN per muscle ring. Implementing these rings as the power source in untethered bio-bots enabled directional locomotion at average speeds of 310 $\mu\text{m/s}$ (1.3 body lengths/min) in response to optogenetic stimulation at 2 Hz. The precise spatiotemporal stimulus provided by optogenetic control also enabled the demonstration of rotation and 2D steering in a muscle-powered device, with average rotational speeds of $2^\circ/\text{s}$ ($120^\circ/\text{min}$). Furthermore, “exercise training” of muscle rings with dynamic optical stimuli and static mechanical stimuli during differentiation resulted in a significant increase in functional performance, with generated forces being $\sim 550\%$ greater in exercised muscle rings compared with a control. These advances in design and

Significance

Understanding the design rules that govern the structure and function of natural biological systems gives us the ability to forward engineer machines integrated with and powered by biological components. Such machines, or “bio-bots,” can sense, process, and respond to dynamic environmental signals in real time, enabling a variety of applications. Here we present a modular optogenetic muscle actuator used to power actuation and locomotion of 3D printed flexible skeletons. Observing and controlling the functional response of such muscle-powered machines helps replicate the complex adaptive functionality we observe in natural biological systems. This demonstration thus sets the stage for building the next generation of bio-integrated machines and systems targeted at a diverse array of functional tasks.

Author contributions: R.R. and R.B. designed research; R.R., C.C., and P.S. performed research; R.R., C.C., S.G.M.U., R.J.P., P.S., and R.D.K. contributed new reagents/analytic tools; R.R. analyzed data; and R.R., C.C., S.G.M.U., P.S., R.D.K., and R.B. wrote the paper.

The authors declare no conflict of interest.

This article is a PNAS Direct Submission.

¹To whom correspondence should be addressed. Email: rbashir@illinois.edu.

This article contains supporting information online at www.pnas.org/lookup/suppl/doi:10.1073/pnas.1516139113/-DCSupplemental.

implementation of modular muscle actuators thus set the stage for building hierarchical multicellular bio-integrated machines and systems for a range of applications. Primary applications in medicine include noninvasive drug delivery and design of dynamic multifunctional implants.

Results

Design and Fabrication of Optogenetic Muscle Ring-Powered Bio-Bots. In vivo, muscle is anchored to bone via tendons, and the concerted contraction of sarcomeres acting in parallel along a muscle fiber drives articulation of bones across joints. We designed and 3D printed a poly (ethylene glycol) diacrylate (PEGDA) hydrogel skeleton composed of two pillars (artificial tendons) that connect the muscle to a flexible beam (articulating joint) to mimic in vivo structure (Fig. S14). We then 3D printed a PEGDA “ring mold” that served as a template for the formation of a muscle ring. To enable comparisons to our previous muscle strip design (10), we also manufactured a strip mold (Fig. 1A).

Optogenetics, the method of genetically engineering light-responsive cells, enables noninvasive external control over cellular function (13). Ion channels that respond to light stimuli have been implemented in a variety of applications that require cellular manipulation. Although the seminal studies in this field were performed on neurons, recent studies have demonstrated optogenetic approaches to control other cell types, including skeletal muscle (12). To implement optogenetic control of our muscle actuators, we used an existing lentiviral transduction protocol to engineer C2C12 murine myoblast cells with a mutated variant of the blue light-sensitive ion channel, Channelrhodopsin-2 (ChR2), namely ChR2(H134R) (Fig. 1B). Transduced cells, labeled with a tdTomato tag, were selected using FACS to maximize expression of ChR2(H134R). Multinucleated myotubes differentiated from these myoblasts were anticipated to demonstrate paced contractility in response to an external light stimulus of 470-nm wavelength.

Optogenetic myoblasts were combined with a solution of Matrigel basement membrane, fibrinogen, and thrombin (Fig. 1C). This cell/gel solution, designed to mimic native extracellular

matrix, was injected into the molds, and traction forces exerted by embedded cells drove self-assembly into densely packed muscle strips and rings (Fig. 1D). Muscle strips formed around (and thus were permanently tethered to) the bio-bot skeletons. Muscle rings were manually transferred to bio-bot skeletons 1 d after seeding (day 1) (Fig. 1E, Fig. S2, and Movie S1). This process allowed for mechanical coupling of the actuator to the device while still preserving modularity of design, because muscle rings could be transferred to any of a wide variety of mechanical skeletons. To simplify manual transfer, bio-bot skeletons were chemically tethered to an underlying glass slide during transfer and mechanically released from the slide on day 2 after seeding. Both muscle strip and ring devices were cultured in growth medium (DMEM + 10% FBS) containing the fibrinolytic inhibitor aminocaproic acid (ACA) for 3 d to induce cell proliferation. They were then transferred to differentiation medium [DMEM + 10% horse serum (HS)] containing ACA on day 4 to drive fusion of individual myoblasts into multinucleated myotubes with mature contractile sarcomeres. This medium was supplemented with human insulin-like growth factor (IGF1) to accelerate the differentiation process and induce muscle hypertrophy (10, 14).

The thickness of engineered muscle tissue is dependent on the formulation of the cell/gel solution. Until a certain lower limit, higher concentrations of cells and fibrin form thinner muscle rings that lead to more densely compacted tissue. Beyond this limit, increasing the cellular and fibrin concentration cannot reduce the muscle tissue thickness further, as the embedded cells and fibrin network occupy a finite volume. The thickness of muscle rings was thus used as a metric to select cell/gel solution formulations that would maximize muscle tissue compactness and cellular density (Fig. 1F and Fig. S3A). This characterization of optimal muscle dimensions coupled with the modularity of the ring design enabled forward engineering of many types of machines including larger scale bio-bots, bio-bots powered by multiple muscle rings, and multilegged bio-bots (Fig. S3 B–D).

Characterization of Optogenetic Muscle Ring Force Output. Macro-scale muscle contraction is the sum of many microscale contractions of individual myotubes acting in parallel. Aligning the axis of contractility for myotubes within muscle is thus critical to observing large combined forces. We performed immunofluorescence staining on muscle rings to observe the distribution of the mature muscle marker, myosin motor protein. A fast Fourier transform (FFT) algorithm was used to determine local alignment (Fig. 2A). Myotubes in muscle rings are aligned at 90° in regions parallel to the bio-bot beam (Fig. 2A-1) and shift in alignment around the edges of the skeleton with smaller peaks at 90° and a larger peak at 45° (Fig. 2A-2) and 135° (Fig. 2A-3), respectively. This analysis reveals a high degree of local alignment along the axis of tension imposed by the mechanical constraint of the bio-bot skeleton.

We performed a closer inspection of muscle ring architecture in the region represented in Fig. 2A-2 via multichannel fluorescence imaging of DAPI cell nucleus marker, the ChR2 tdTomato tag, and the immunostained myosin marker (Fig. 2B). Cells were evenly distributed throughout the muscle ring and expressed the tdTomato marker for optogenetic ion channels, indicating that they could be expected to generate functional contractile responses to blue light stimulation. Scanning electron microscopy imaging likewise showed densely compacted and evenly distributed myotubes with a high degree of local alignment (Fig. 2C). A cross-section image of the muscle ring was used to verify that hierarchical organization of muscle architecture and alignment was preserved in 3D (Fig. 2D).

To measure the passive tension force exerted by both muscle strip and muscle ring devices, we used Euler-Bernoulli beam bending theory to correlate bio-bot skeleton deformation with muscle force production. On average, passive tension forces for muscle strip and ring devices were not significantly different, with muscle strips exerting passive tension forces of $1,940 \pm$

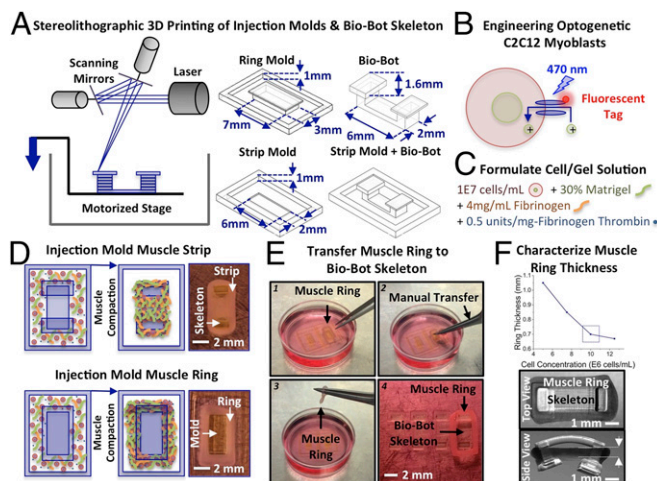


Fig. 1. Design and fabrication of optogenetic muscle ring-powered bio-bots. (A) Stereolithographic 3D printing is used to fabricate ring and strip injection molds and bio-bot skeletons from a PEGDA photosensitive resin. (B) C2C12 myoblasts are engineered to incorporate a mutant variant of the blue-light sensitive cation channel, Channelrhodopsin-2, in the cell membrane. The ion channel is tagged with a red fluorescent tdTomato tag. (C) Optogenetic myoblasts embedded within a natural hydrogel matrix. (D) Injection molding of cell/gel solution into muscle strip and ring molds. (E) Manual transfer of muscle rings from the injection mold to the bio-bot skeleton (Movie S1). (F) Optimization of muscle ring thickness as a function of cell concentration.

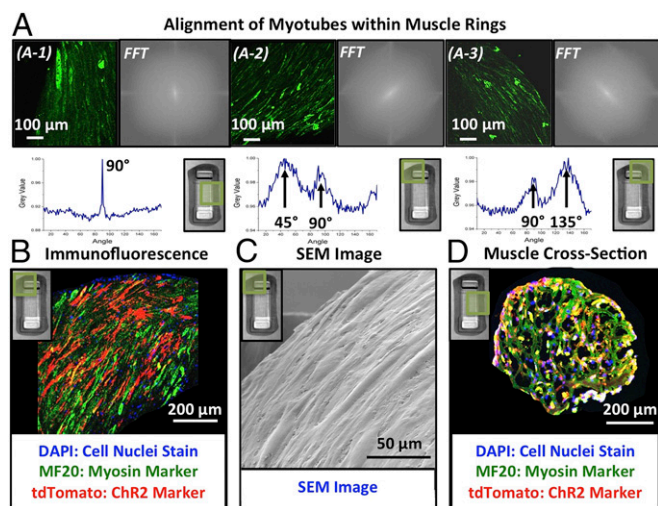


Fig. 2. Characterization of muscle ring architecture. (A) Alignment of myotubes within various regions of muscle rings assessed via FFT analysis of fluorescent myosin marker. Fluorescence image (Upper Left), FFT (Upper Right), and normalized gray value of the FFT as a function of angle (Lower Left) are presented for three regions of muscle rings, shown as green highlights on a whole device (Lower Right). (B) Multichannel fluorescence imaging of DAPI cell nucleus marker, the optogenetic ChR2 tdTomato tag, and the MF-20 myosin marker imaged via confocal fluorescence microscopy and presented as a merged 3D stack. (C) Scanning electron microscopy image of muscle ring surface. (D) Cross-section of fluorescently immunostained muscle ring, showing uniform distribution of mature functional myotubes throughout the entire cross-section.

350 μN and muscle rings exerting passive tension forces of $1,710 \pm 230 \mu\text{N}$ on day 9 after seeding (Fig. S4A). This force corresponds to a passive tension stress of $1.6 \pm 0.3 \text{ kPa}$ for muscle strips, which had average cross-sectional areas of $1.2 \pm 0.04 \text{ mm}^2$ ($n = 3$), and $3.2 \pm 0.4 \text{ kPa}$ for muscle rings, which had had average cross-sectional areas of $0.54 \pm 0.06 \text{ mm}^2$ ($n = 3$). These stress values are comparable to those previously reported for tissue engineered skeletal muscle (10, 12, 15).

Mature muscle was stimulated optically and electrically using custom-built apparatus (Fig. 3A), and a Kelvin-Voigt viscoelasticity model was used to correlate contraction-induced displacement of bio-bot skeletons to active tension forces produced by engineered muscle. Optical stimulation of muscle strip and ring devices at 1, 2, and 4 Hz with 50-ms pulses produced paced contractions (Fig. S4B) and physiological force-frequency response behavior (Fig. 3B-1 and C-1), where the dynamic fluctuation of active tension force reduced with increasing frequency. As with native skeletal muscle at high frequency stimulation, the passive tension baseline increased during the stimulation period, indicating that the muscle was not allowed to fully relax from one received stimulus before the next received stimulus. For muscle strips, forces produced by optical stimulation (45 ± 11 , 32 ± 12 , and $25 \pm 12 \mu\text{N}$ at 1, 2, and 4 Hz, respectively) are significantly lower (Fig. 3B-2) than those produced by electrical stimulation (195 ± 19 , 112 ± 26 , and $88 \pm 30 \mu\text{N}$ at 1, 2, and 4 Hz, respectively). By contrast, there was no significant difference between optical and electrically stimulated active tension forces in muscle rings (Fig. 3C-2). At stimulation frequencies of 1, 2, and 4 Hz, optical stimulation of rings produced active tension forces of 195 ± 7.3 , 114 ± 8.1 , and $110 \pm 16 \mu\text{N}$, respectively, whereas electrical stimulation produced active tension forces of 185 ± 17 , 117 ± 19 , and $119 \pm 6.7 \mu\text{N}$.

This difference in functional performance of optogenetic muscle strips and rings is explained by an analysis of the effective penetration depth (500–740 μm) of 470-nm light into biological tissue (16, 17). Although muscle strips had maximum thicknesses up to 1,200 μm , the densely compacted muscle ring actuators were less than 700 μm thick (Fig. 1D). Hence, light stimulation of

muscle rings excited a larger number of myotubes than in muscle strips, resulting in greater force production. This principle was verified by demonstrating that increasing light energy density increased muscle ring functional performance (Fig. S4C). A maximum energy density of 1.9 mW/mm^2 was used for all experiments, a value that falls within the range of saturation intensity values reported in the literature on optogenetic cells (12, 18, 19). Electrical stimulation of muscle strips and rings revealed comparable active tension force production for both designs, indicating that similar numbers of myotubes were recruited in each case (Fig. S4D). When normalized by cross-sectional area, however, muscle rings produced significantly greater active

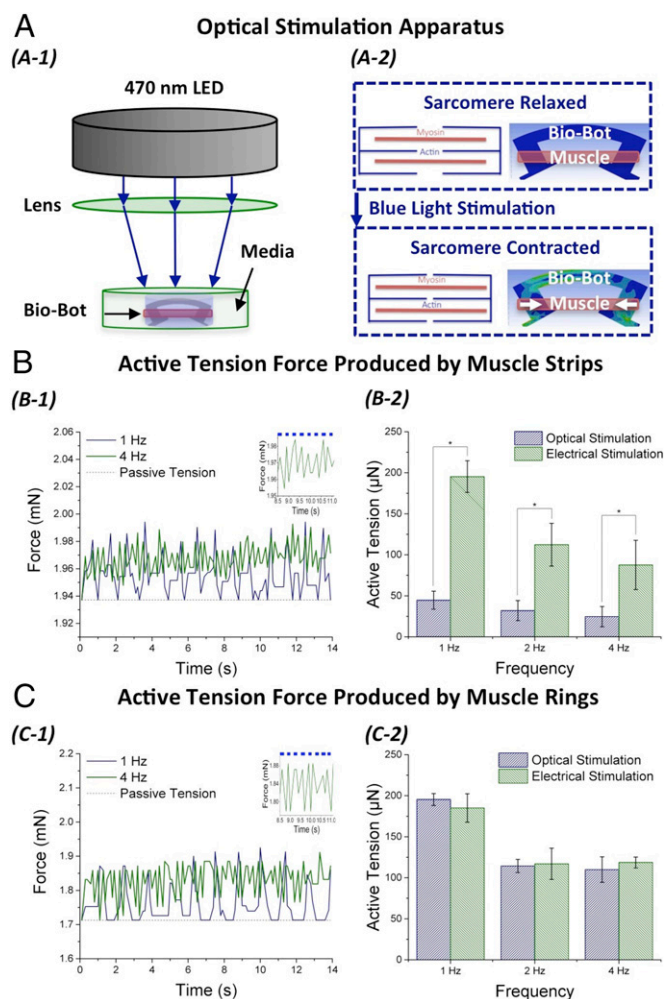


Fig. 3. Optically stimulated actuation of muscle strips and rings. (A) Apparatus used to optically stimulate engineered muscle. (A-1) 470-nm light is focused on to bio-bots at a maximum intensity of 1.9 mW/mm^2 . (A-2) At the microscale, light stimulation induces contraction of individual myotubes. The coordinated contraction of several sarcomeres produces observable macro-scale contraction. (B) Active tension force produced by muscle strips (day 12). (B-1) Active tension force tracked over time for a representative muscle strip. Inset of 4-Hz stimulation over 2 s shown for clarity, with a dashed blue line indicating the stimulus pulse train. (B-2) Active tension force compared between optical and electrical stimulation of muscle strips ($P < 0.05$, $n = 3$, one-way ANOVA, post hoc Tukey test). (C) Active tension force produced by muscle rings (day 12). (C-1) Active tension force tracked over time for a representative muscle ring. Inset of 4-Hz stimulation over 2 s shown for clarity, with a dashed blue line indicating the stimulus pulse train. (C-2) Active tension force compared between optical and electrical stimulation of muscle rings ($P < 0.05$, $n = 3$, one-way ANOVA, post hoc Tukey test). All data are presented as mean \pm SD.

tension stresses with a maximum of 0.34 ± 0.03 kPa at 1-Hz stimulation compared with muscle strips, which produced active tension stresses of only 0.16 ± 0.02 kPa.

Optimizing Functional Performance of Optogenetic Muscle Rings. “Exercise training” of engineered muscle during differentiation has been shown to increase force output. For electrically stimulated conditioning, improved functionality is attributed to increased differentiation, improved alignment, and increased glucose uptake (20, 21). For mechanically stimulated conditioning, improved functionality is attributed to a change in gene regulation and protein expression, increased metabolic activity, cellular proliferation, and improved myofiber organization (10, 22).

A previous study has shown that optical stimulation during differentiation of optogenetic C2C12s in 2D can improve the alignment of sarcomeric proteins and increase the fraction of contractile myotubes (23). We hypothesized that optical conditioning of muscle rings during differentiation could thus lead to an enhancement in functional performance (force production). The mechanism of periodic cellular depolarization and contraction would be similar to that of electrical stimulation, but less invasive, as it avoids electrolysis of the surrounding media. Furthermore, we hypothesized that combining mechanical and optical stimulation could lead to synergistic enhancements in functional performance.

To provide a passive mechanical stimulus during differentiation, we kept bio-bots chemically tethered to an underlying glass slide throughout differentiation to maximize cellular alignment and myotube formation. Bio-bots were mechanically released from the stiff underlying substrate before stimulation. To provide optical conditioning during differentiation, we subjected muscle rings to a daily regimen of optical stimulation at 1, 2, and 4 Hz. We measured active tension force output for four different groups: control group 1, no mechanical conditioning (bio-bots released from substrate on day 1), no optical conditioning; control group 2, mechanical conditioning (bio-bots tethered to substrate until day 12), no optical conditioning; exercise group 1, no mechanical conditioning, optical conditioning during differentiation (days 4–11); and exercise group 2, mechanical conditioning, optical conditioning (Fig. 4A).

An analysis of force output for exercise group 1 revealed that active tension forces grew from 56 ± 11 μ N on day 7 (the first day with observable macroscale contractility) to 195 ± 24 μ N on day 12 at 1-Hz stimulation (Fig. 4B-1). By contrast, control group 1 produced active tension forces of only 43 ± 6.0 μ N on day 12. Control group 2 produced forces of 91 ± 37 μ N on day 12. Although these forces were higher than those of bio-bots from control group 1, the results were not significantly different. Exercise group 2, which was subjected to both mechanical and optically stimulated exercise during differentiation, produced active tension forces of 283 ± 32 μ N on day 12 (Fig. 4B-2 and Movie S2). These data serve to demonstrate that mechanically and optically stimulated exercise can lead to significant improvements in muscle functional performance, and the combination of both types of stimuli synergistically enhances force output even further. This result is consistent with previous demonstrations of mechanical and electrical multimodal stimulation for engineered muscle (24, 25) but is the first demonstration, to our knowledge, of optical conditioning driving functional improvements in muscle performance. As optical stimulation provides a less invasive and cell type-specific approach for localized control of muscle contraction, this approach to enhancing functional performance is a significant improvement over the current state of the art.

To validate our hypothesis that optical stimulus conditioning improves myotube formation, we assessed the DNA and protein content in control group 2 and exercise group 2 muscle rings and compared the ratio of protein/DNA in each case. Larger protein/DNA ratios are correlated with greater cellular hypertrophy (15). As all rings contained the same number of embedded myoblasts, the DNA content for all muscle rings was 1.76 ± 0.35 μ g DNA/mg muscle. However, the protein content for exercise group 2 rings

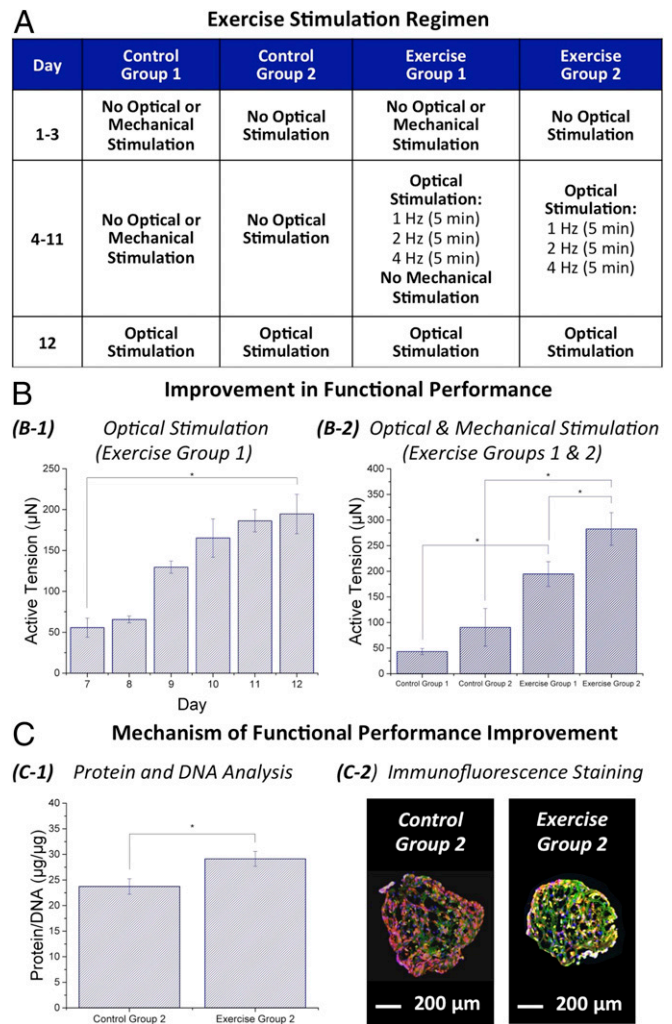


Fig. 4. Functional performance optimization via exercise training. (A) Exercise stimulation regimen for four experimental groups during growth (days 1–3) and differentiation (days 4–11) (Fig. S2). Force output in response to optical stimulation is compared on day 12. (B) Improvement of muscle functional performance in response to optical conditioning. (B-1) Active tension produced by exercise group 1 assessed from days 7 to 12 ($P < 0.05$, $n = 3$, one-way ANOVA, post hoc Tukey test). (B-2) Active tension comparison between all four experimental groups (Movie S2) ($P < 0.05$, $n = 3$, one-way ANOVA, post hoc Tukey test). (C) Assessment of mechanisms underlying functional performance improvement. (C-1) Ratio of protein content to DNA content measured for control group 2 and exercise group 2 ($P < 0.05$, $n = 4$, one-way ANOVA, post hoc Tukey test). (C-2) Immunofluorescence stained cross-sections of exercise group 2 and control group 2, showing visibly greater expression of myosin marker in exercised muscle rings. All data are presented as mean \pm SD.

was 51.2 ± 2.6 μ g protein/mg muscle, compared with 41.7 ± 2.7 μ g protein/mg muscle for control group 2. The ratio of protein/DNA was thus significantly larger in the exercise conditioned case, 29.1 ± 1.5 μ g protein/ μ g DNA compared with the control group, 23.7 ± 1.5 μ g protein/ μ g DNA, corroborating the theory that exercise conditioning resulted in increased cellular hypertrophy (Fig. 4C).

Directional Locomotion and 2D Steering in Optogenetic Muscle Ring-Powered Bio-Bots. Because the most readily observable form of work produced by an actuator is locomotion, this was chosen as the desired functional output for our muscle-powered machines. First, to observe directional (1D) locomotion in response to optical stimulation, the design of the bio-bot skeleton was made asymmetric by increasing the length of one of the hydrogel pillars. With each contraction of the engineered muscle tissue, the

Incorporating optogenetic ion channels into muscle rings provided us with a noninvasive method of exciting groups of aligned myotubes with precise spatiotemporal control. Compared with previously presented approaches, which controlled muscle-powered bioactuators via electrodes in close proximity to the bio-actuator device, optogenetics provided noncontact yet localized control of stimulation. This fundamental distinction drove complex controllable directional locomotion and 2D steering of bio-bots, a capability that has not been previously presented in untethered biological machines powered by engineered muscle. This design modification, enabled by targeted genetic engineering of skeletal muscle myoblasts, thus resulted in a profound improvement in the complexity of functional behaviors produced by engineered muscle. An important advancement presented in this study is the improvement in functional performance produced by exercise training of muscle rings with combined optical and mechanical stimuli. This evidence of increased muscle force production in response to multimodal conditioning demonstrates the dynamically tunable and adaptive nature of these modular bioactuators.

Conclusions

Forward engineered biological machines harness the ability of biological materials to sense, process, and respond to environmental signals in real time. The modular bioactuators we present in this study power bio-bots that demonstrate adaptive behavior in response to noninvasive light stimuli, enabling a variety of applications that require dynamic sensing and actuation. This type of adaptive behavior, which emerges from the coordinated

interactions in a multicellular network, drives much of the complex functionality we observe in natural biological systems (26). Future generations of bio-bots could further harness the power of biological materials by incorporating self-assembling or self-healing functionalities or serving as factories of cell-secreted factors. Incorporating multiple cell types, such as neurons for signal processing or endothelial cells for vascularization and nutrient transport, would enable the design and fabrication of more complex biological machines. As many such machines will require modular bioactuators, this demonstration of a light-controlled adaptive skeletal muscle-powered biological machine thus enables a variety of applications while simultaneously setting the stage for the next generation of bio-integrated machines and systems.

Methods

Information on design and fabrication of 3D printed optogenetic muscle-powered bio-bots and quantification of functional performance all appear in *SI Methods*.

ACKNOWLEDGMENTS. We thank Prof. Taher Saif and Brian Williams from University of Illinois at Urbana-Champaign (UIUC) and Prof. H. Harry Asada from Massachusetts Institute of Technology for technical discussions, and Dr. Mayandi Sivaguru from UIUC for assistance with confocal imaging. This work was funded by National Science Foundation (NSF) Science and Technology Center Emergent Behavior of Integrated Cellular Systems (EBICS) Grant CBET-0939511. R.R. was funded by NSF Graduate Research Fellowship Grant DGE-1144245 and NSF Cellular and Molecular Mechanics and Bionanotechnology (CMMB) Integrative Graduate Education and Research Traineeship (IGERT) at UIUC (Grant 0965918).

- Griffith LG, Naughton G (2002) Tissue engineering—Current challenges and expanding opportunities. *Science* 295(5557):1009–1014.
- Harrison RH, St-Pierre J-P, Stevens MM (2014) Tissue engineering and regenerative medicine: A year in review. *Tissue Eng Part B Rev* 20(1):1–16.
- Kamm RD, Bashir R (2014) Creating living cellular machines. *Ann Biomed Eng* 42(2):445–459.
- Egan P, Moore J, Schunn C, Cagan J, LeDuc P (2015) Emergent systems energy laws for predicting myosin ensemble processivity. *PLOS Comput Biol* 11(4):e1004177.
- Chan V, Asada HH, Bashir R (2014) Utilization and control of bioactuators across multiple length scales. *Lab Chip* 14(4):653–670.
- Carlsen RW, Edwards MR, Zhuang J, Pacoret C, Sitti M (2014) Magnetic steering control of multi-cellular bio-hybrid microswimmers. *Lab Chip* 14(19):3850–3859.
- Feinberg AW, et al. (2007) Muscular thin films for building actuators and powering devices. *Science* 317(5843):1366–1370.
- Nawroth JC, et al. (2012) A tissue-engineered jellyfish with biomimetic propulsion. *Nat Biotechnol* 30(8):792–797.
- Chan V, et al. (2012) Development of miniaturized walking biological machines. *Sci Rep* 2:857.
- Cvetkovic C, et al. (2014) Three-dimensionally printed biological machines powered by skeletal muscle. *Proc Natl Acad Sci USA* 111(28):10125–10130.
- Neal D, Sakar MS, Ong L-L, Harry Asada H (2014) Formation of elongated fascicle-inspired 3D tissues consisting of high-density, aligned cells using sacrificial outer molding. *Lab Chip* 14(11):1907–1916.
- Sakar MS, et al. (2012) Formation and optogenetic control of engineered 3D skeletal muscle bioactuators. *Lab Chip* 12(23):4976–4985.
- Deisseroth K (2011) Optogenetics. *Nat Methods* 8(1):26–29.
- Vandenburgh HH, Karlisch P, Shansky J, Feldstein R (1991) Insulin and IGF-I induce pronounced hypertrophy of skeletal myofibers in tissue culture. *Am J Physiol* 260(3 Pt 1):C475–C484.
- Hinds S, Bian W, Dennis RG, Bursac N (2011) The role of extracellular matrix composition in structure and function of bioengineered skeletal muscle. *Biomaterials* 32(14):3575–3583.
- Barolet D (2008) Light-emitting diodes (LEDs) in dermatology. *Semin Cutan Med Surg* 27(4):227–238.
- Moreira MC, Prado R, Campos A (2011) Application of high brightness LEDs in the human tissue and its therapeutic response. *Applied Biomedical Engineering*, eds Gargiulo GD, McEwan A (InTech, Rijeka, Croatia), pp 3–20.
- Klapoetke NC, et al. (2014) Independent optical excitation of distinct neural populations. *Nat Methods* 11(3):338–346.
- Bryson JB, et al. (2014) Optical control of muscle function by transplantation of stem cell-derived motor neurons in mice. *Science* 344(6179):94–97.
- Duffy RM, Feinberg AW (2014) Engineered skeletal muscle tissue for soft robotics: Fabrication strategies, current applications, and future challenges. *Wiley Interdiscip Rev Nanomed Nanobiotechnol* 6(2):178–195.
- Donnelly K, et al. (2010) A novel bioreactor for stimulating skeletal muscle in vitro. *Tissue Eng Part C Methods* 16(4):711–718.
- Powell CA, Smiley BL, Mills J, Vandenburgh HH (2002) Mechanical stimulation improves tissue-engineered human skeletal muscle. *Am J Physiol Cell Physiol* 283(5):C1557–C1565.
- Asano T, Ishizuka T, Morishima K, Yawo H (2015) Optogenetic induction of contractile ability in immature C2C12 myotubes. *Sci Rep* 5:8317.
- Rangarajan S, Madden L, Bursac N (2014) Use of flow, electrical, and mechanical stimulation to promote engineering of striated muscles. *Ann Biomed Eng* 42(7):1391–1405.
- Liao I-C, Liu JB, Bursac N, Leong KW (2008) Effect of Electromechanical Stimulation on the Maturation of Myotubes on Aligned Electrospun Fibers. *Cell Mol Bioeng* 1(2-3):133–145.
- Macklem PT (2008) Emergent phenomena and the secrets of life. *J Appl Physiol* (1985) 104(6):1844–1846.